ACS Combinatorial Science

Research Article

pubs.acs.org/acscombsci

Optical High-Throughput Screening for Activity and Electrochemical Stability of Oxygen Reducing Electrode Catalysts for Fuel Cell Applications

C. Dogan, K. Stöwe, and W. F. Maier*

Lehrstuhl für Technische Chemie, Universität des Saarlandes, Gebäude C4 2, 66123 Saarbrücken, Germany

Supporting Information

ABSTRACT: A fluorescence-based electro-optical high-throughput method and setup for testing the oxygen reduction reaction (ORR) activity and electrochemical stability of 60 materials in parallel is described. We present thus a quantitative method for activity measurements for ORR-catalysts by optical fluorescence data acquisition. The fluorescence behavior of fluorescein, phloxine B, and umbelliferone as indicators is presented. The effect of oxygen concentration, saturation, and supply on electrochemical response is presented. Corrections for internal resistance differences and intensity differences are described. The final method allowed position independent determination of activities on the working-electrode library, containing up to 60 different electrocatalysts. A total of 378 selected mixed oxides have been studied. Cu/Ni/Mn and Co/Ni/Mn oxides proved electrochemically most active and comparable to a Pt-containing reference catalyst.

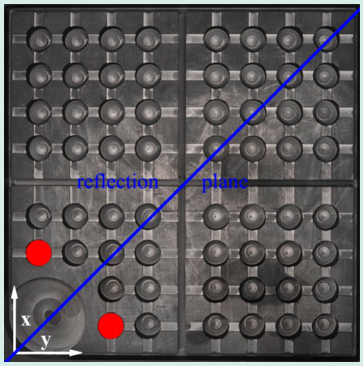

KEYWORDS: *optical, high-throughput-screening, ORR catalysts, fluorescent indicators, electrochemical stability*

1. INTRODUCTION

1.1. The Cathodic Oxygen Reduction Reaction (ORR). Fuels cells are environmentally friendly and low-pollution devices that generate electric power by converting the chemical energy of a fuel directly into electrical.[1,2] However, due to the poor catalytic performance of standard cathode materials in the reduction of oxygen and the high costs of the constituents, the commercialization of fuel cells is still restricted.[3,4] Because of its unique catalytic properties, Pt or Pt supported on carbon (Pt/C) is the most widely used catalyst for ORR.[5] Nevertheless, even the best commercially available Pt catalyst leads to an energy loss of about 30%.[6] The high complexity and the sluggish kinetics due to the stability of the O_2 molecule represent the main challenges of the ORR.[7,8] At the cathode, two different oxygen reduction processes are possible.[8−16] Thereby, oxygen can be reduced directly by four electrons to water (eq 1), or it can be reduced in an indirect two-electron pathway. The indirect reduction of oxygen is less complex, and initially hydrogen peroxide is produced (eq 2), which either can diffuse away from the electrode or can be further reduced to water (eq 3) in a second step.

$$O_2 + 4H^+ + 4e^- \leftrightarrows 2H_2O \qquad E_0 = 1.23\ V \qquad (1)$$

$$O_2 + 2H^+ + 2e^- \leftrightarrows H_2O_2 \qquad E_0 = 0.68\ V \qquad (2)$$

$$H_2O_2 + 2H^+ + 2e^- \leftrightarrows 2H_2O \qquad E_0 = 1.77\ V \qquad (3)$$

To avoid catalyst corrosion by peroxide and to obtain maximum efficiency, catalysts that reduce oxygen directly to water are desired.

1.2. Principle of the Optical Activity Determination of Catalysts. The principle of optical electrode catalyst activity screening, reviewed in ref 22, was first published in 1998 by Reddington et al.[17] The authors utilized a quinine containing electrolyte to visualize the methanol oxidation reaction (MOR) activity of an inkjet printed ternary Pt−Rh−Os library on carbon paper. Dependent on methanol conversion, the quinine electrolyte developed a fluorescence intensity caused by an increase of the pH-value of the electrolyte used to qualitatively compare electrode performance.[17,18] This screening method was adapted[19,20] with the objective of optimization with regard to signal quantification. In both cases, the optical systems consisted of an UV lamp for fluorescence excitation and a CCD camera for recording the fluorescence intensity. The electrochemical system of the setup was comprised of a typical three electrode arrangement consisting of working, counter, and reference electrodes. Welsch et al. applied a 150 mm × 150 mm sized graphite plate as working electrode with 60 individual sample wells, connection channels, and the reference electrode compartment.[19] The working electrode plate was connected to the potentiostat by a copper foil. Using an electrolyte bridge consisting of five individual conducting paths, the reference and working electrode compartment was spatially separated from the counter electrode on the one hand, and on the other hand the electrolyte resistance between both compartments was reduced to a minimum. For the elimination of stray light

Received: August 12, 2014
Revised: December 6, 2014
Published: January 2, 2015

DOI: 10.1021/co500128m
ACS Comb. Sci. 2015, 17, 164−175

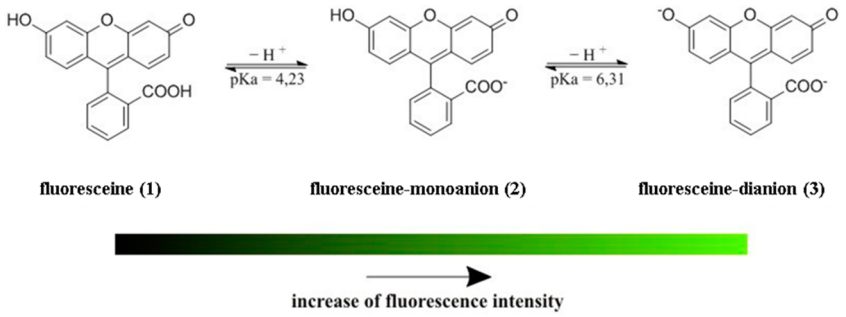

Figure 1. Molecular structure of fluoresceine and its anions responsible for fluorescence, as well as the corresponding schematic fluorescence intensity development under UV excitation.[23−27]

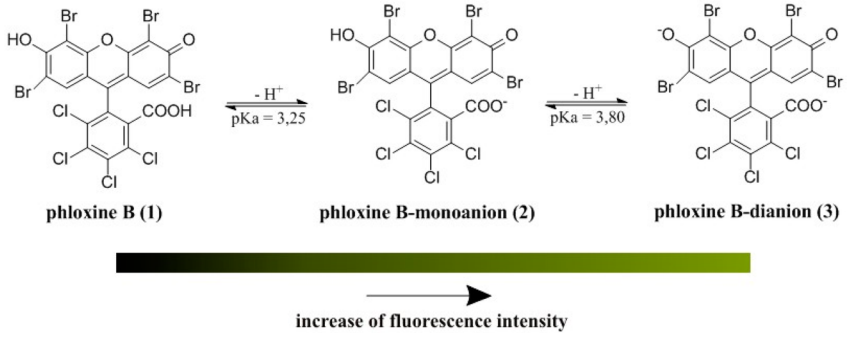

Figure 2. Molecular structure of phloxine B and its anions responsible for fluorescence, as well as the corresponding schematic fluorescence intensity development under UV excitation.[29−31]

sources, all components were enclosed in a light-tight wooden box. This setup permitted the parallel screening of 60 catalysts for MOR using a quinine containing electrolyte. In contrast to Reddington et al., the high-throughput setup of Welsch et al. allowed the quantification of investigated catalysts due to the restriction of fluorescent dye diffusion into neighboring sample compartments.

Based on the optical method for the detection of methanol oxidation catalysts[17,19,20] fluorescent indicator systems for ORR detection were developed. As basis the work of Liu et al.[21] adding fluoresceine to the applied electrolyte for screening the activity of Pt and non-Pt based catalysts was adopted. But in this approach the reference, counter, and working electrolyte were dipped in a joint electrolyte making quantification of catalyst activity difficult for diffusion reasons.

1.3. Fluorescence Indicators for Optical ORR Detection. The optical detection of catalyst activities for ORR requires a change in fluorescent properties of one component in the electrolyte, which first and foremost depends on the fluorescent indicator used. A protonation or deprotonation associated with a change in the pH-value of the indicator solution leads to a change of the absorption properties of the fluorescent dye under excitation with UV light. The optically verifiable fluorescent species allows the quantification of the reaction considered.

Because the ORR is associated with a proton consuming process (see eq 1), a fluorescent indicator is needed that reveals fluorescence with increasing pH value.[22] The fluorescent properties of fluoresceine change by stepwise deprotonation of the neutral molecule to its mono- and dianion responsible for the fluorescence of fluoresceine.[21,23−25] Figure 1 shows the basic molecular structure and the anions of fluoresceine revealing fluorescence intensity. Phloxine B was also reported as a fluorescent indicator for ORR screening applications. Chen et al.[28] applied phloxine B to screen bifunctional catalysts for regenerative fuel cells. Phloxine B also changes its fluorescence upon increase of the pH value. In Figure 2, the basic molecular structure of phloxine B and its derivates responsible for fluorescence are shown. Under UV-light excitation, the reddish mono- and dianions of phloxine B under normal light change into a yellowish green fluorescence. Umbelliferone represents another fluorescence dye used to determine the enzymatic activity of β-glucuronidase.[32] The blue colored fluorescence of umbelliferon is attributed to the monoanion formed by deprotonation (see Figure 3). Park et al. have been using fluoresceine as optical indicator in ORR-studies with modified Pt-catalysts and have been working under a constant oxygen atmosphere.[33]

2. EXPERIMENTAL SECTION

2.1. Fluorescence Indicator Properties. One liter of a 0.25 μM fluoresceine, phloxine B, and umbelliferone (7-hydroxycoumarin) solution was placed in the mixer unit of the automatic titration system (Methron) and the solution was

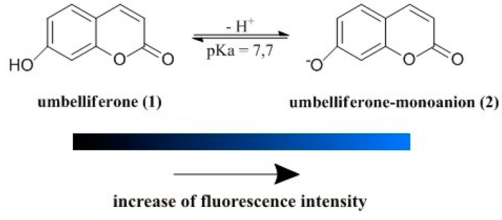

Figure 3. Molecular structure of umbelliferone and its anion responsible for fluorescence as well as the corresponding schematic fluorescence intensity development under UV excitation.[35−38]

DOI: 10.1021/co500128m
ACS Comb. Sci. 2015, 17, 164−175

adjusted to a pH of 10 with 1 M sodium hydroxide solution. The titrator was adjusted so that the fluorescence indicator solutions were titrated to a pH of 3 in 0.5 pH steps by 1 M sulfuric acid solution. After the desired pH was achieved, 15 mL of the indicator solution was transferred to another vessel and served for further characterization. To reduce dilution effects, the indicator solutions with pH values larger than 10 and smaller than 3 were adjusted with concentrated sodium hydroxide and sulfuric acid, respectively. Until characterization, the solutions prepared were wrapped with aluminum foil and stored in dark to avoid exposure to light. The fluorescence indicator properties of the indicator solutions prepared were analyzed with an UV/vis microtiter plate reader (Biotek PowerWave XS). Each indicator solution (300 μL) was added to a well of the 96 well microtiter plate, and the UV/vis spectra were recorded in the range of 200−700 nm.

The UV stability of the fluorescent indicators was tested with a 254 nm UV lamp (2 × 8 W, Benda) placed over the fluorescent indicator containing microtiter plate at a distance of 6 cm. The bottom of the microtiter plate was cooled with a polystyrene box filled with ice, reducing evaporation of the 300 μL fluorescent indicator solutions. The solutions were exposed to UV light for 1 and 3 h. After the contact time specified, the microtiter plate was removed, and the UV/vis spectra of the fluorescent indicator solutions were repeatedly recorded in the range of 200−700 nm.

2.2. Notation and Synthesis of Compounds. A simplified notation is used to specify the materials examined: the composition of a binary mixed oxide is generally described as $A_aB_bO_x$ and a ternary mixed oxide as $A_aB_bC_cO_x$, whereby x describes the unknown oxygen content of the compounds. A, B, and C stand for particular elements, and the a, b, and c describe the molar fractions of the elements in mol % (adding up to 100 mol %), not accounting for the oxidation states of the elements in the compositions and thus not for oxide molar fractions, since these may vary depending on treatment and environment.

Mixed oxides were synthesized by a modified sol−gel process as described previously.[19,20] The stock solutions were prepared dissolving 0.25 M precursor in a 1:1 (v/v) mixture of isopropanol (Sigma-Aldrich) and propionic acid (Sigma-Aldrich). All precursors used are specified in Table 1. The planning and control of the syntheses were carried out with the software Plattenbau[34] and the help of a pipetting robot (MultiProbe II EX Packard). The stock solutions were mixed in 1.5 mL GC vials according to the ratios of the elements in the composition intended. After mixing, the samples were placed in an orbital shaker (Titramax 100, Heidolph) for 1 h and dried for 2 days at room temperature and then for 8 days at 40 °C. The mixed oxides were obtained after calcination of the dried gels under static air at 250 and 400 °C, respectively, for 5 h (heating rate 30 °C/h).

In total, 378 mixed oxides were synthesized, containing 231 binary compositions $A_aB_bO_x$ with a = 2, 5, 10, 25, 50, 75, and 98 mol %. The remaining 147 had ternary compositions $A_aB_bC_cO_x$ with a = 16.7, 33.3, or 66.7 mol %, b = 16.7, 33.3, or 66.7 mol %, and $c = 100 - (a + b)$ mol %. The compositions $Cu_aNi_bMn_cO_x$ were additionally synthesized in the range a = 10, 20, 40, 60, or 80 mol %, b = 10, 20, 40, 60, or 80 mol %, and $c = 100 - (a + b)$ mol %.

2.3. Coating of Working Electrode Spots. *2.3.1. Mixed Oxides and PtO_x.* Five milligrams of each mixed oxide prepared as described above was dispersed in a mixture of ethylene glycol and water (7:3 (v/v); mass concentration, 0.5 mg/30 μL) for 5 min using an ultrasonic bath (MK 100, Bandelin). Thirty microliter of the dispersions was pipetted directly from the dispersion vial positioned in the ultrasonic bath to the catalyst support area on the working electrode (WE) array. The removal of the ethylene glycol/water mixture was carried out in a vacuum oven at room temperature for 1 h at 0.2 bar followed by 16 h at ~10^{-3} mbar. After drying of the catalyst coatings, 10 μL of a 0.05% Nafion solution in isopropanol (Standard, 5% Nafion 117 solution, Sigma-Aldrich) was pipetted on top of each of the catalyst coatings and dried for 20 min in an argon flow.

2.3.2. Pt/C. Pt/C (8.0−8.5 mg; Pt content 19.1 wt %) was sonicated in a 1.5 mL GC vial with a mixture of Nafion (5% Nafion 117 solution, Sigma-Aldrich) and water (1:9 (v/v); mass concentration, 0.5 mg/30 μL) for several minutes. The catalyst−Nafion−water mixture was treated under high vacuum conditions for 10 min to remove air or other gases from the pores of the catalyst. Therefore, the crimped GC vials were connected via a canula unit to a vacuum pump. Thirty microliter of the dispersions was pipetted onto the catalyst support area on the working electrode array followed by drying the catalyst coating in an oven at 70 °C for 30 min. Subsequently 10 μL of 5% Nafion solution was pipetted on top of each catalyst coating and dried for 10 min in an oven at 70 °C.

The resulting coatings were rinsed with water for 5 h by filling the wells of the working electrode with 500 μL of deionized water to allow the Nafion to reach its swelling state. Before the measurements, the water was removed by the use of a water-driven pump.

2.4. Fluorescence Based High-Throughput Screening. The electrolyte solution for fluorescence based measurements was composed of 25 μM fluoresceine (Sigma-Aldrich) and 0.2 M sodium sulfate (Sigma-Aldrich) in deionized water (Elga Purelab UVF, Elga Labwater). For the activity measurements, the electrolyte was purged for 20 min with pure oxygen (4.5 Praxair, 450 mL min^{-1}) to obtain an oxygen saturated solution. The electrochemical stability tests were carried out by purging the electrolyte with argon to obtain an oxygen-free solution. The fluorescence emission was recorded under UV lamp

Table 1. Precursors Used for Mixed Oxide Syntheses

element	precursor	molecular formula
Mo	molybdenum acetate (dimer)	$Mo_2C_8H_{12}O_8$
Co	cobalt acetate tetrahydrate	$CoC_4H_6O_4{\cdot}4H_2O$
Bi	bismuth acetate	$BiC_6H_9O_6$
Ga	gallium acetylacetonate	$GaC_{15}H_{24}O_6$
V	vanadium triisopropoxy oxide	$VC_9H_{21}O_4$
In	indium acetylacetonate	$InC_{15}H_{21}O_6$
Mn	manganese acetate dihydrate	$MnC_6H_9O_6{\cdot}2H_2O$
Ce	cerium acetate	$CeC_6H_9O_6$
Sm	samarium acetate	$SmC_6H_9O_6$
Pr	praseodymium acetate trihydrate	$PrC_6H_9O_6$
Cu	copper acetate	$CuC_4H_6O_4$
Ni	nickel acetate tetrahydrate	$NiC_4H_6O_4{\cdot}4H_2O$
Al	aluminum acetate	$AlC_6H_9O_6$
Fe	iron acetate	$FeC_4H_6O_4$
Nb	niobium ethoxide	$NbC_{10}H_{25}O_5$
Ta	tantalum ethoxide	$TaC_{10}H_{25}O_5$
Cr	chromium acetate dimer monohydrate	$Cr_2C_8H_{12}O_8{\cdot}2H_2O$
Zr	zirconium-*n*-propoxide	$ZrC_{12}H_{28}O_4$
Ti	titanium isopropoxide	$TiC_{12}H_{28}O_4$

DOI: 10.1021/co500128m
ACS Comb. Sci. 2015, 17, 164−175

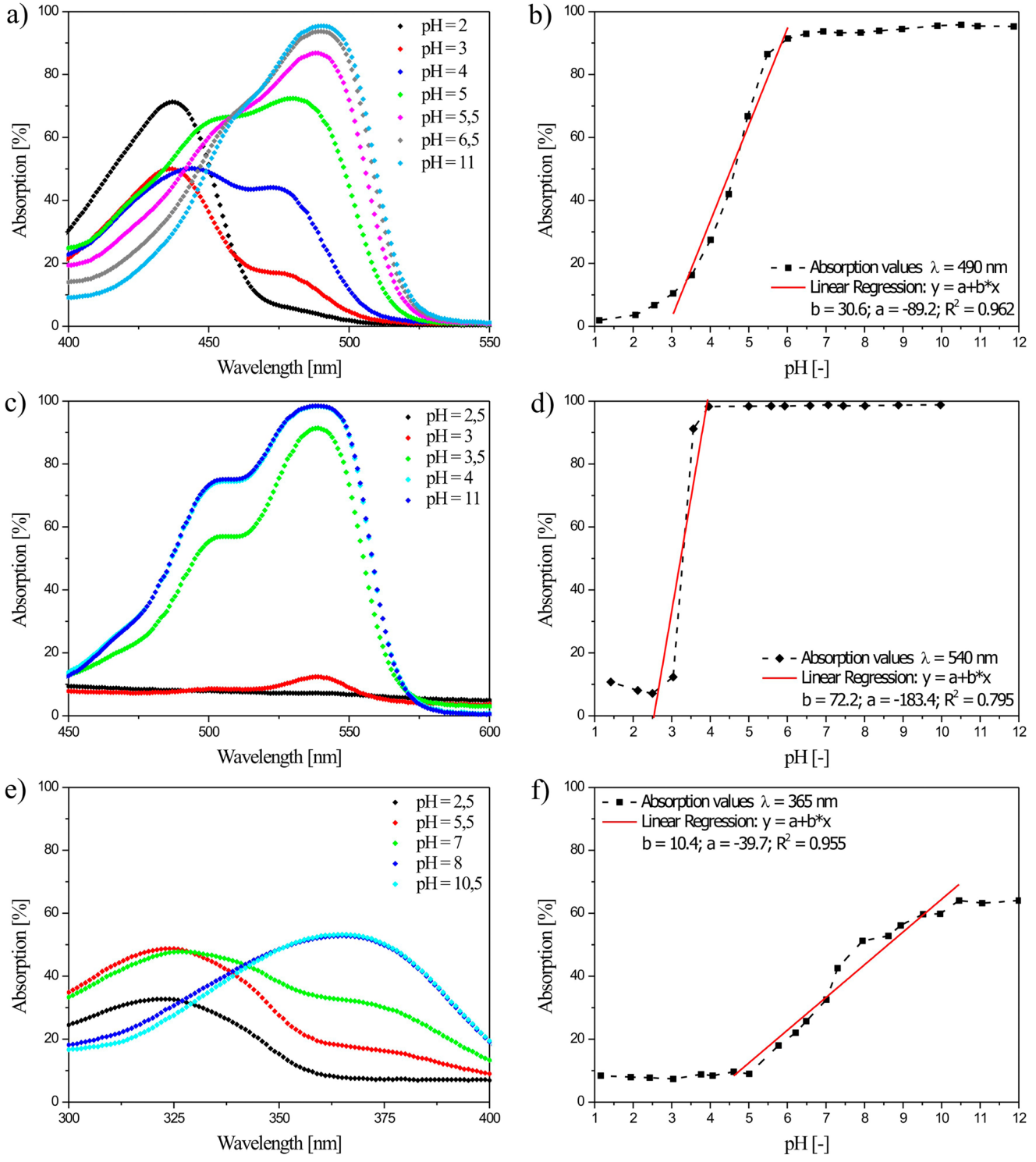

Figure 4. pH dependencies of absorption spectra (a, c, e) and pH dependent absorption behavior (b, d, f) of a 25 μM solution of (a, b) fluoresceine, (c, d) phloxine B, and (e, f) umbelliferone in the relevant wavelength maximum range, λ_{max}, of each fluorescent indicator.

excitation at a wavelength of 254 nm (VL-215 C, 30W, Vilber Lourmat). A potentiostat was used to control the potential of the WE array compartments (PP 220, Zahner Elektronik).

High-throughput fluorescence intensity measurements were performed with the whole setup enclosed by a tailor-made light-tight wooden box. A digital high-resolution monochrome 12-bit CCD camera (Retiga 4000 R, Q Imaging) equipped with lens (TAM 25-HB/12, Tamron) and band elimination filter (E 420 LP, Chroma Technology Corp.) was positioned perpendicular to the plane of the graphite plate WE array. The UV lamp was placed next to the camera lens to ensure a uniform illumination of the WE array. A copper foil positioned below the WE array was used to ensure a good electrical contact of the graphite plate to the potentiostat. Reproducible contact and exact positioning of the WE array toward the camera were guaranteed by two location screws in combination with a positioning aid. The light-tight wooden box was attached to an external ventilation, reducing temperature changes of the

DOI: 10.1021/co500128m
ACS Comb. Sci. 2015, 17, 164−175

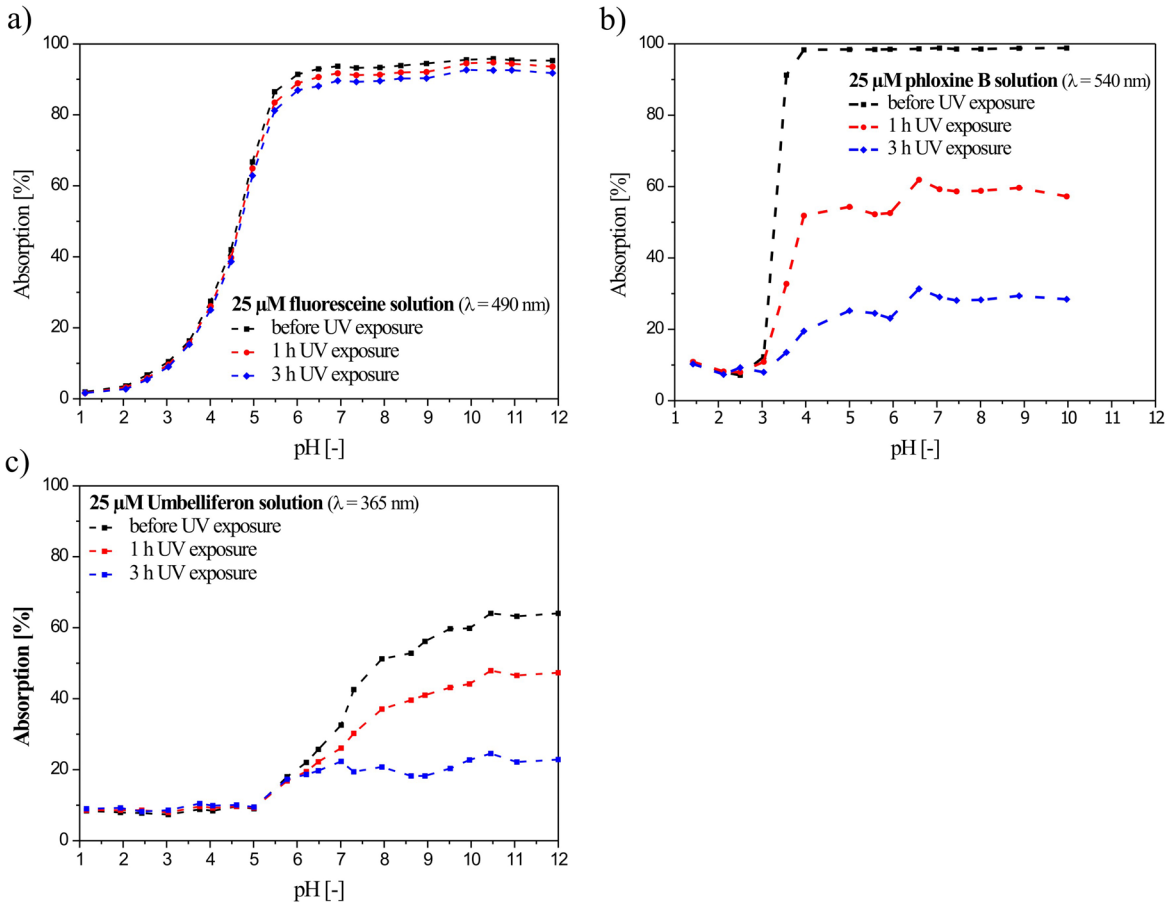

Figure 5. pH dependent absorption behavior of a 25 μM solution of (a) fluoresceine, (b) phloxine B, and (c) umbelliferone before and after UV light (254 nm) exposure for 1 and 3 h.

CCD sensor, which allowed an undisturbed detection of the fluorescence intensity during the measurements. A platinum net acting as counter electrode (CE) was separated from the Hg/$HgSO_4$ reference electrode (RE, ref 621, Radiometer Analytical)/WE compartment by five separate salt bridges (see also Figures 7–9). The whole WE compartment including CE with salt bridges was embedded in a gastight enclosure sealed by a circumventing O-ring with an UV transparent quartz glass plate lid. By purging this electrode compartment with oxygen, we guaranteed a constant oxygen concentration in the electrolyte solution. Images were automatically acquired and processed using a PC and commercial imaging software (Image Pro Plus, Media Cybernetics). The potentiostat was controlled by a tailor-made Labview application. For catalyst screening, the WE array was set to a constant potential of 50 mV vs SHE, and images were obtained repeatedly after a time interval of 30 s over a reaction time of 40 min. Additionally, an image for background subtraction was acquired at the beginning of each data acquisition series. Using *Image-Pro Plus* software, we defined 60 areas of interests (AOI) in each image according to well positions. A bitmap analysis for each AOI was applied. The summation of the greyscale values obtained for each pixel was realized using a commercial spreadsheet calculation software resulting in intensity values with arbitrary units for each well and potential, respectively. For data analysis, the intensity values, I_{AOI}, were plotted against the testing time. The corresponding equations and detailed description of intensity values calculations have been published in previous articles.[19,20,22] The automation of data analysis was achieved by the use of a macro software tool (*MacroTools Works*, Pitrinec Inc.).

3. RESULTS AND DISCUSSION

3.1. Development of an Optical ORR High-Throughput Screening Method. *3.1.1. Fluorescence Properties and UV Stability of Fluoresceine, Phloxine B, and Umbelliferone.* To establish a correlation between absorption and emission spectra of the fluorescent indicator solutions, the position of the absorption maxima of the dyes in fluorescing state in the UV/vis spectra were of outmost importance. In the case of fluoresceine, phloxine B, and umbelliferone, the mono- or dianions of the indicators are responsible for the fluorescence. By deprotonation or protonation of the fluorescent indicator, bathochromic or hypsochromic wavelength shifts are observed for the absorption maxima depending on the dye. The pH dependencies of the UV/vis spectra of a 25 μM fluoresceine, phloxine B, and umbelliferone solution in a wavelength range of 200–700 nm are shown in Figure 4a,c,e (bathochromic effects; hypsochromic effect with increasing pH, for instance, for quinine). To get a better overview, only selected spectra at some pH values are shown. The evaluation of the pH dependent absorption values at constant λ_{max} wavelength of the fluorescent indicator enables applicability evaluation for optical ORR detection. The slope of the linear regression (Figure 4b,d,e) of the absorption maximum intensity at λ_{max} as a function of pH gives a direct measure for the fluorescence

DOI: 10.1021/co500128m
ACS Comb. Sci. 2015, 17, 164–175

sensitivity of the indicator. Since the ORR is accompanied by proton consumption, the fluorescent indicator should reveal a high slope value over a large pH range, preferentially in acid to neutral regime.

In case of fluoresceine (Figure 4a) the absorption maxima at different pH were obtained in the visible wavelength range, λ_{max}, from 437 to 490 nm.[24,25] The maximum wavelength of 490 nm already was reached at pH = 6.5, which did not change anymore by further increase until pH = 12. From the absorption versus pH diagram (Figure 4b) the largest change in absorption (at λ_{max} of 490 nm) was reached in the pH range of 3 to 6; at pH values greater 6.5, the absorption remained constant. With an acid constant pK_a = 6.31 (see Figure 1) for the monoanion−dianion equilibrium, the dianion of fluoresceine is the predominant and fluorescing species in solution in this pH range. The linear plot of the absorption change range revealed slope values of 30%/pH unit representing a high sensitivity of the indicator. To apply fluoresceine as indicator for optical determination of the ORR activity of a material the initial pH value of the fluoresceine solution should be 3.5 to obtain optimal screening conditions. The high sensitivity as well as broad pH range of fluorescence intensity change preferentially in the acid regime permits a qualitative and quantitative determination of the ORR activity of materials by applying fluoresceine solution as indicator.

The absorption maxima of the phloxine B solutions at various pH values (pH = 3−12) was located also in the visible wavelength range of 530−540 nm (Figure 4c). Phloxine B solutions with pH < 3 were colorless, and their UV/vis spectra did not show a maximum in the visible wavelength range.[39] Only at pH > 3 did the absorption reach a maximum at λ_{max} of 540 nm with a rather sudden change at pH = 3.5 (pK_a = 3.25 and 3.80, see Figure 2) . Further pH increase of the phloxine B solutions did not result in a significant absorption intensity change, which suggests that again the dianion form of phloxine B is dominating in solution. The linear slope in the absorption change region between a pH of 3 and 4 was calculated as 72%/pH unit representing the very high sensitivity of phloxine B (Figure 4d). But sensitivity is not the only decisive factor. Because the high fluorescence intensity change of phloxine B in a small pH range of 3−4 does not allow a susceptible activity differentation of a material (only an "active" or "inactive" predicate could be assigned in this case), this dye was disregarded for the further setup developments.

The absorption maxima of the umbelliferone solutions were located below the visible wavelength range between 327 and 365 nm (Figure 4e), which is responsible for the colorless appearance of the solution.[32,37,40] A distinct absorption change was observed in the pH range of 5 to 10, which permits a quantitative activity differentation. The low slope value of 10%/pH unit at a moderate intensity change represents a less sensitive as well as less susceptible fluorescent indicator system than fluoresceine or phloxine B. To ultilize umbelliferone as fluorescent indicator the initial pH, should be adjusted between 5 and 5.5 (Figure 4 f).

Due to the application of an UV lamp during the activity measurements, the fluorescent indicators should show utmost stability against UV degradation within the measuring time range. Figure 5a,b,c presents the absorption behavior of a 25 μM solution of fluoresceine, phloxine B, and umbelliferone before and after UV light (254 nm) treatment, respectively. Evaluation of UV light stability was determined by comparing the steepest ascents in the absorption intensity plot of each fluorescent indicator as a function of pH. Consequently a large decrease in the slope values indicates a decomposition of the fluorescent species and represents an instable fluorescent indicator. Both phloxine B (Figure 5 b) and umbelliferone (Figure 5 c) exhibited instability against UV exposure. Compared with the solution of phloxine B before exposure the absorption-slope values of irradiated solutions decreased from 72%/pH unit to nearly one-half after 1 h irradiation time, and after an irradiation time of 3 h, only one-tenth of the initial slope value was observed (Table 2). A similar decomposition rate of the umbelliferone sample was obtained. In contrast, fluoresceine exhibited a sufficient stability against UV irradiation within exposure time. Even after an irradiation time of 3 h, an insignificant alteration of the initial absorption-slope value of 30%/pH unit was recognized (Figure 5a). On that account, only fluoresceine was verified as a fluorescent indicator for optically based determination of material activities for ORR. This confirms the selection of fluoresceine for ORR-reduction studies reported earlier.[33,41]

Table 2. Linear Slope Values for Phloxine B, Fluoresceine and Umbelliferone before and after a UV Light Treatment in the Inflection Point Absorption Range (Steepest Ascent) of Each Fluorescent Indicator

indicator solution	UV exposure (h)	slope b
fluoresceine		30.64
	1	29.90
	3	29.25
phloxine B		72.15
	1	30.78
	3	7.19
umbelliferon		10.90
	1	7.24
	3	1.76

3.1.2. Optimization of the Fluorescing Dye Containing Electrolyte. Based on the specifications proposed by Liu et al.,[21] the electrolyte was composed of fluoresceine as fluorescing indicator, sodium sulfate to increase electrical conductivity, and dissolved oxygen as reactant. To optimize the catalytic activity optical determination of a material, adjustments of fluorescence indicator concentration, initial electrolyte pH value, oxygen saturation concentration in the electrolyte, and wavelength of the excitation source were essential. Thereby, keeping constant the saturation of oxygen in the electrolyte during the high-throughput measurements represented the major challenge.

As already noted,[22] a lower basic fluorescence background intensity of fluoresceine was achieved by using a 254 nm UV lamp leading to a more sensitive optical visualization of the fluorescence changes in the electrolyte used. Additionally the fluorescent dye concentration studies revealed that the best fluorescence intensity variation was detected using a 25 μM fluoresceine electrolyte solution. Referring to Figure 4b, the initial pH value of the electrolyte should be near to 3.5 to obtain the highest intensity change anticipating that absorption and fluorescence intensity are directly correlated. To eliminate ORR catalyst screening interference by reactant depletion, the initial oxygen content of 4.2 mg L^{-1} in the electrolyte was increased by feeding additional oxygen at 250 mL min^{-1} through the quartz lid covered three electrode cell assembly. Figure 6a illustrates the electrolyte oxygen concentration as a function of purging time. After a purging time of 20 min, the

DOI: 10.1021/co500128m
ACS Comb. Sci. 2015, 17, 164−175

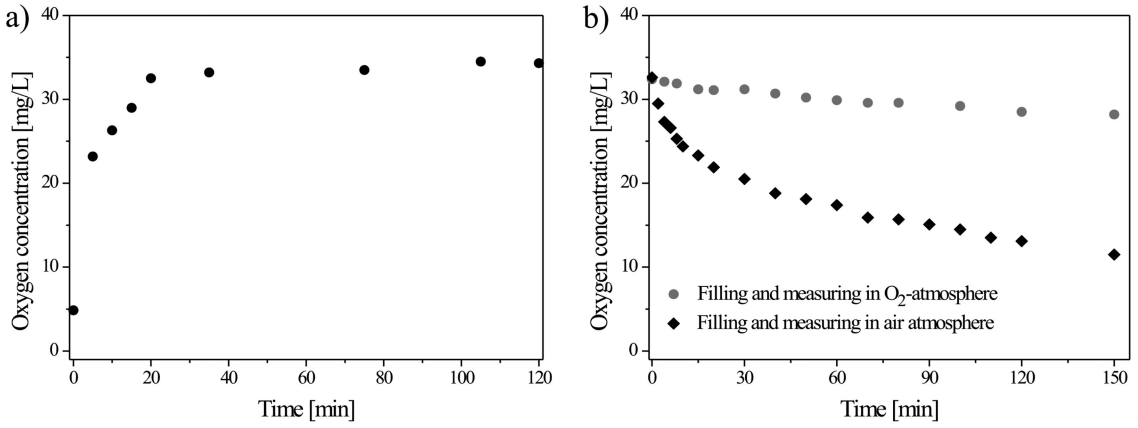

Figure 6. (a) Dissolved oxygen concentration of a 25 μM fluorescein electrolyte as a function of oxygen purging time after filling in air and (b) temporal oxygen concentration change of the electrolyte by filling and measuring in oxygen and in air atmosphere.

initial oxygen content of 4.2 mg L^{-1} was enhanced by 95% to 32.5 mg L^{-1}. Because further purging did not increase the oxygen content significantly, a purging time of 20 min was regarded as sufficient for activity measurements. To test the influence on the results of different gas atmospheres during catalyst screening, oxygen saturated fluoresceine electrolyte was filled in the graphite plate in air and alternatively under an oxygen atmosphere established by a glovebag surrounding the cell assembly with permanently flowing oxygen. In Figure 6b, the time dependent oxygen concentration of the electrolyte in both atmospheres is shown. During the measurements in air, a decrease of the saturated electrolyte from 32.5 to 11.5 mg L^{-1} was received, while filling and measuring in an oxygen atmosphere resulted in a less distinct decrease in oxygen content (29.6 mg L^{-1}).

3.1.3. High-Throughput Setup for Fluorescence Intensity Measurements. Based on the setup published by Welsch et al. for methanol oxidation reaction (MOR) catalyst screening,[19,20] as well as the results described above, a high-throughput setup for a parallel quantitative ORR catalyst activity determination was developed. The setup consists of a tailor-made light-tight wooden box equipped with an optical unit (CCD camera, UV lamp) and a standard three-electrode electrochemical unit. The filling of the WE array with an oxygen-saturated fluoresceine containing electrolyte as well as measurement of the ORR catalyst activity in a constantly renewed oxygen atmosphere had to be realized by this setup. Thereby the whole electrode compartment was encapsulated by a gastight wooden frame. Vents incorporated in the frame permitted oxygen supply as well as the electrical contact of RE and WE array to the potentiostat. With the help of a glovebag unit, the WE array was filled with the oxygen presaturated electrolyte and the salt bridges were positioned under a permanent oxygen flow. A schematic representation of the setup for filling the WE in oxygen atmosphere is shown in Figure 7. Subsequently, the glovebag unit was replaced by a quartz plate as lid with a circumferential O-ring as sealing within a few seconds. By means of an aerator mounted on top of the setup, the temperature was kept constant during the activity measurements. The schematic high-throughput setup to determine the ORR catalyst activity is presented in Figure 8.

The adaption of the optical screening system originally designed for MOR screening to an electrolyte containing fluoresceine as indicator for ORR testing was performed according to Welsch et al.[20] Following this procedure, an

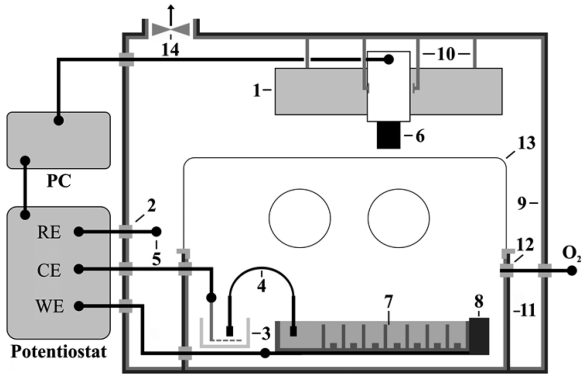

Figure 7. Schematic representation of the high-throughput setup for filling the working electrode in a flowing oxygen atmosphere: (1) UV lamp, (2) light-tight feedthroughs, (3) counter electrode (CE) container with CE, (4) salt bridges, (5) reference electrode (RE), (6) CCD camera, (7) working electrode (WE) graphite plate, (8) WE positioning aid, (9) light-tight box, (10) holders for lamp and camera, (11) wooden frame, (12) gas feeding, (13) glovebag unit, (14) aerator.

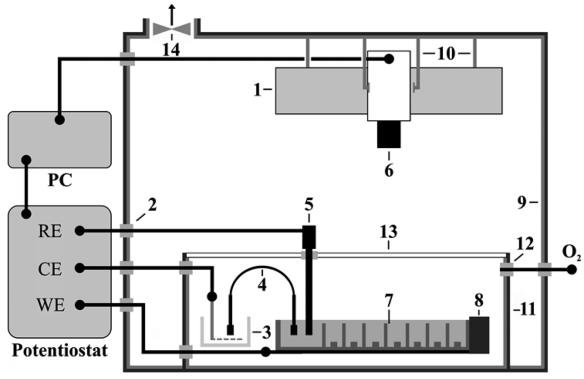

Figure 8. Schematic representation of the high-throughput setup for ORR catalyst activity testing: (1) UV lamp, (2) light-tight feedthroughs, (3) container with CE, (4) salt bridges, (5) RE, (6) CCD camera, (7) WE plate, (8) WE positioning aid, (9) light-tight box, (10) holders for lamp and camera, (11) wooden frame, (12) gas feeding, (13) quartz plate, (14) aerator.

exposure time of 320 ms and average correcting factors, k_m, depending on the well position $x-y$ on the WE array were provided. For the intensity correction of the 60 well positions

DOI: 10.1021/co500128m
ACS Comb. Sci. 2015, 17, 164−175

due to their different geometrical positions relative to the excitation source, a standard deviation of 1% was obtained.

3.1.4. Effect of Electrolyte Internal Resistance and Validation of the High-Throughput Screening System. Due to the structural design of the graphite plate WE assembly (see Figure 9) and the resulting different distances of the 60 well positions from the RE, different internal resistances of the electrolyte were obtained for each well position. According to eq 4, the well position-dependent electric resistance of the electrolyte solution can be calculated from the concentration-dependent electrolyte resistivity, ρ.

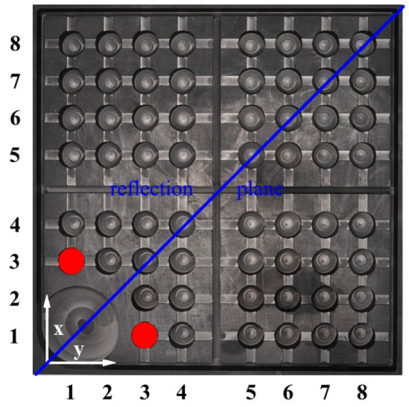

Figure 9. Design of the high-throughput graphite plate WE array with its 60 well positions (x–y coordinates), connection channels, and the RE array; red dots indicate reference positions 3–1 and 1–3; blue line indicates mirror plane emphasizing symmetric arrangement of wells drilled into the graphite plate.

$$R = (\rho l(x\text{—}y))/A \quad (4)$$

Because of approximately the same electrode area size A of all 60 positions, the individual resistance R is dependent only on the specific distance $l(x$–$y)$ between the well position and the RE. Thereby higher resistances R were achieved by increasing distances l. In Figure 9, the high-throughput graphite plate WE design with the 60 well positions is shown. The well positions 1–3 and 3–1 (marked by red dots) owning the smallest distance to the RE represent the reference position for further consideration.

To enable materials activity rankings in a setup with position-dependent resistances, the internal resistance effect has to be eliminated either by increasing the amount of the conducting salt[21] in the electrolyte or by implementation of mathematical correction factors. To examine the impact of conducting salt amount, the WE was coated 60 times with 0.5 mg of a carbon supported platinum catalyst (Pt/C, Pt content 19.1 wt %) and the evolutions of the fluorescence intensity of each position were compared in 0.2 and 0.4 M Na_2SO_4 containing fluoresceine electrolytes. Figure 10 illustrates the temporal fluorescence intensity evolution of the Pt/C coated reference position 3–1 and the average fluorescence intensity evolution for the remaining 58 positions in the different Na_2SO_4 and fluoresceine containing electrolytes. All 58 positions showed a lower fluorescence intensity compared with the reference position 3–1. Both electrolytes resulted in significant differences of the 58 sample positions compared with the reference position 3–1 with a standard deviation of 60% for the 0.2 M Na_2SO_4 and 27% for the 0.4 M Na_2SO_4 electrolyte, respectively. Under these conditions, the parallel detection of activities of 60 materials could not be determined with satisfying quality. Consequently, the internal resistance effect had to be compensated implementing mathematical correction factors for each vial position. Consequently, for each vial position, an electrolyte resistance correction factor, k_E, was calculated. After the correction, the fluorescent intensities of the 58 vial positions were directly related to the fluorescent intensity of the reference position 3–1.

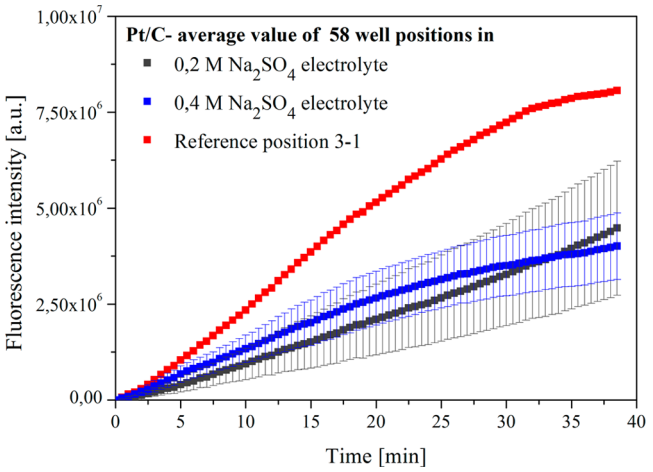

Figure 10. Temporal fluorescence intensity evolution of Pt/C coated positions; red, reference position 3–1; blue and gray, average fluorescence intensity evolution with corresponding error bars of the remaining 58 positions in a 0.2 and 0.4 M Na_2SO_4 and fluoresceine containing electrolyte, respectively.

To illustrate the effect of correction factor application, some well positions on the working electrode were coated again with 0.5 mg of Pt/C catalyst and the temporal fluorescence intensity evaluation was recorded. Coating the reference, middle, and edge positions on the working electrode array permits a comparison and predicate on the fluorescence evaluation behavior of the working plate. In Figure 11, the average fluorescence intensity and the standard deviation of the coated positions with and without consideration of the correction factors are illustrated. Without electrolyte resistance correction

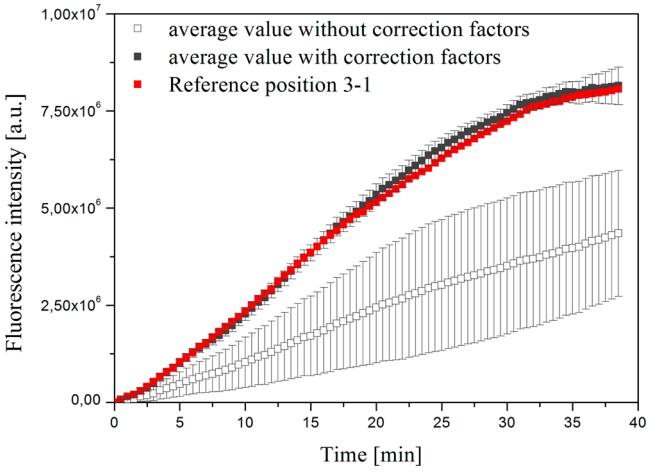

Figure 11. Average fluorescence intensity evaluation and the standard deviations of some Pt/C coated positions with and without considering the correction factors.

DOI: 10.1021/co500128m
ACS Comb. Sci. 2015, 17, 164–175

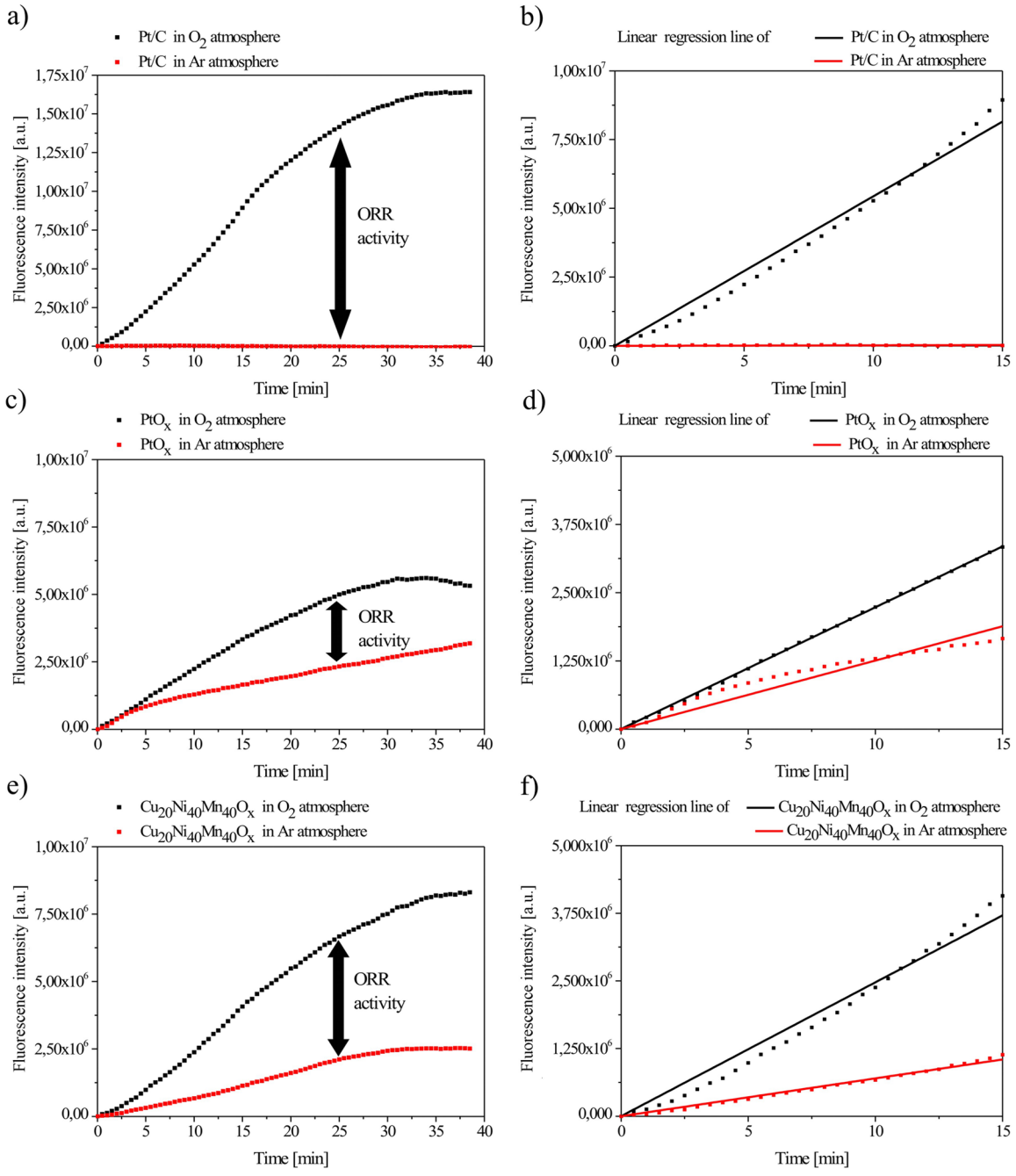

Figure 12. Fluorescence intensity evolution of Pt/C, PtO_x, and $Cu_{20}Ni_{40}Mn_{40}O_x$ catalysts under oxygen and argon conditions with corresponding linear regression line; black dots, $I^k_{AOI,total}$, red dots, $I^k_{AOI,res}$.

factors, k_E, a high standard deviation of 60% was calculated, which was reduced to 5% with correction factors.

3.2. High-Throughput Electrochemical Stability Screening and Determination of the ORR Activity. Due to the acidic environment of the proton conducting Nafion layer used in the activity measurements, the applied catalysts should be stable against dissolution (leaching) in mineral acids of high concentration. All mixed oxides used in this work were tested for acid stability according to the high-throughput prescreening method already described previously.[22] Thereby, 172 of the 378 total synthesized mixed oxides exhibited leaching stability against a 1 M sulfuric acid. But this acid prescreening method did not consider the influence on electrochemical parameters, such as the applied voltage. Thus, a voltage impact could also result in decomposition of the catalyst and can be described formally by salt formation according to eq 5.

$$MO_x + 2xHX \rightarrow MX_{2x} + xH_2O \quad (5)$$

The acid HX represents the proton conductive Nafion layer used. Proton consumption due to mixed oxide dissolution leads to a shift in pH value of the fluoresceine electrolyte and contributes to the evolution of fluorescence intensity. Accordingly, the quantified total fluorescent intensity $I^k_{AOI,total}$ during activity measurements is composed of the ORR

DOI: 10.1021/co500128m
ACS Comb. Sci. 2015, 17, 164−175

fluorescence intensity, $I^{k}_{AOI,ORR}$, and the fluorescence intensity of catalysts dissolving under the voltage applied, $I^{k}_{AOI,res}$ (eq 6).

$$I^{k}_{AOI,total} = I^{k}_{AOI,ORR} + I^{k}_{AOI,res} \quad (6)$$

The fluorescent intensity $I^{k}_{AOI,res}$ can be determined by fluorescence recording of the material under oxygen absence. Consequently, ORR active and electrochemically stable catalysts should reveal fluorescence intensity only in the presence of oxygen and should not develop fluorescence intensity in absence of oxygen.

First of all, the total fluorescent intensities $I^{k}_{AOI,total}$, of all 174 acid stable mixed oxides were determined. Thereby, 130 mixed oxides developed no fluorescence, 39 mixed oxides developed a low fluorescence intensity, and the mixed oxides $Cu_{20}Ni_{40}Mn_{40}O_x$, $Co_{66}Cu_{17}Mn_{17}O_x$, and $Co_{66}Ni_{17}Mn_{17}O_x$ developed a high fluorescence intensity, $I^{k}_{AOI,total}$ comparable to or slightly higher than the reference material platinum oxide PtO_x. Accordingly these last three mixed oxides were regarded as hits and further investigated. The results of the fluorescence measurements of all 174 mixed oxides are summarized in the Supporting Information.

For determination of the electrochemical stability of Pt/C, PtO_x, $Cu_{20}Ni_{40}Mn_{40}O_x$, $Co_{66}Cu_{17}Mn_{17}O_x$, and $Co_{66}Ni_{17}Mn_{17}O_x$ the temporal fluorescence intensity evolution of the catalysts was initially tested by using an argon purged 25 μM fluoresceine electrolyte in an argon atmosphere. The measurements were carried out at constant voltage of 50 mV vs SHE. Subsequently, the catalytic activities of the catalysts were tested under oxygen flow conditions. In Figure 12, the fluorescence intensity evolution behavior of the Pt/C, PtO_x, and $Cu_{20}Ni_{40}Mn_{40}O_x$ catalysts in oxygen and in argon conditions are compared. In argon atmosphere, the reference material Pt/C did not show any fluorescence intensity evolution over the measuring period. Fluorescence intensity was only observed under flowing oxygen, demonstrating the catalytic activity of Pt/C (Figure 12a). Thus, Pt/C represents an active and electrochemically stable catalyst. PtO_x (Figure 12c), as well as $Cu_{20}Ni_{40}Mn_{40}O_x$ (Figure 12e), showed fluorescence even in the absence of oxygen, indicating electrochemical instability.

To generate real data for comparisons, ORR activity values corrected for array position as well as dissolution effects had to be defined. Note that for fluorescence measurements in the absence of oxygen the slope b of the linear regression (eq 7) of the fluorescence intensity was regarded as a measure for the electrochemical stability of the catalyst. The slope calculated from the fluorescence intensity evolution in an oxygen atmosphere (eq 8) represents the oxygen reducing ability and electrochemical stability of the catalysts. Consequently, the difference value, b_{ORR} (eq 10) can be used for comparing the ORR activity of catalysts. In Figure 12b,d,f, the linear regression lines of the Pt/C, PtO_x, and $Cu_{20}Ni_{40}Mn_{40}O_x$ catalysts are illustrated, and the asocciated slope values b_{total} and b_{res} are listed in Table 3.

Ar atmosphere:

$$I^{k}_{AOI,res}(t) = b_{res}t \quad (7)$$

O_2 atmosphere:

$$I^{k}_{AOI,total}(t) = b_{total}t \quad (8)$$

$$I^{k}_{AOI,ORR} = I^{k}_{AOI,total} - I^{k}_{AOI,res} \quad (9)$$

Table 3. Slope Values, b_{total} and b_{res}, Determined by Linear Regression of the Fluorescence Intensity Evolution and the Calculated Slope Values, b_{ORR}

	slope ($\times 10^4$)		
catalyst	b_{total}	b_{res}	b_{ORR}
Pt/C	54.4	0	54.4
PtO_x	22.3	12.6	9.7
$Cu_{20}Ni_{40}Mn_{40}O_x$	24.7	7.0	17.7
$Co_{66}Ni_{17}Mn_{17}O_x$	18.6	13.2	5.4
$Co_{66}Cu_{17}Mn_{17}O_x$	21.2	11.8	9.4

$$b_{ORR} = b_{total} - b_{res} \quad (10)$$

A b_{ORR} value of 17.7×10^4 min^{-1} was received for the compound $Cu_{20}Ni_{40}Mn_{40}O_x$, which represents the most ORR active mixed oxide of this study. However, the activity of $Cu_{20}Ni_{40}Mn_{40}O_x$ was three times lower than that of the reference material Pt/C with $b_{ORR} = 54.4 \times 10^4$ min^{-1}. But compared with platinum oxide PtO_x, which was synthesized by the same method as the mixed oxides, the compound $Cu_{20}Ni_{40}Mn_{40}O_x$ offered an even better real ORR activity and the compound $Co_{66}Cu_{17}Mn_{17}O_x$ offerred comparable real ORR activity.

4. SUMMARY AND CONCLUSIONS

A fluorescence-based, electro-optical high-throughput method and setup for testing the ORR activity and electrochemical stability of 60 materials in parallel was developed. The fluorescence behavior of the indicator solutions of fluoresceine, phloxine B, and umbelliferone were investigated. A high fluorescence sensitivity as well as a large pH range of fluorescence intensity change and a sufficient stability against UV irradiation were only obtained with fluoresceine. To identify the catalytic activity of materials optically, the fluoresceine electrolyte was optimized in terms of fluoresceine concentration, starting electrolyte pH value, and oxygen saturation in the electrolyte. The natural oxygen content of the electrolyte was almost doubled by oxygen purging for 20 min. To keep dissolved oxygen gas saturated in the electrolyte during the activity measurements filling and measuring in a flowing oxygen atmosphere was necessary. Any internal resistance effects caused by the structural design of the working electrode plate were compensated by implementation of mathematical correction factors. After application of this correction the high-throughput setup allowed the determination of position-independent acivities of the materials on the WE library.

To discover new Pt-free ORR materials based on mixed oxides, a high-throughput approach incorporating a sol−gel process was used. All 378 mixed oxides prepared in this work were tested for acid stability, and 172 of these exhibited stability against 1 M sulfuric acid. ORR activity tests revealed three mixed oxides, $Cu_{20}Ni_{40}Mn_{40}O_x$, $Co_{66}Cu_{17}Mn_{17}O_x$, and $Co_{66}Ni_{17}Mn_{17}O_x$, with activities comparable to the Pt-reference catalyst. To verify the stability of these mixed oxides toward applied potential, a reactant-free electrolyte was used in the fluorescence-based high-throughput method. All three mixed oxides showed electrochemical instability detected by the comparison of fluorescence intensity data in different gas environments. Thus, we present here for the first time a quantitative method for real activity measurements by optical fluorescence data acquisition corrected for electrochemical

DOI: 10.1021/co500128m
ACS Comb. Sci. 2015, 17, 164−175

instabilities caused by dissolution of the materials to be tested. This emphasizes the challenge set by the acidic environment of the PEMFC. Consequently, other Pt-free ORR active catalysts reported in literature, for instance, the perovskites, can only be applied in alkaline or neutral media as in AFC, SOFC, or metal/air batteries. To meet the media challenge, actual and future research on Pt-free ORR PEMFC catalysts is almost entirely focused on carbon derivatives such as graphene and N-modified carbon.

■ ASSOCIATED CONTENT

Supporting Information

Slope values b_{total} of binary mixed oxides and of ternary mixed oxides determined by linear regression of the fluorescent intensity evolution. This material is available free of charge via the Internet at http://pubs.acs.org.

■ AUTHOR INFORMATION

Corresponding Author

*Tel: +496 81 302 2422. E-mail address: w.f.maier@mx.uni-saarland.de.

Notes

The authors declare no competing financial interest.

■ ACKNOWLEDGMENTS

The authors thank Umicore AG & Co. KG for support and D. Herein and A. Reichel for discussions.

■ REFERENCES

(1) Jijil, C. P.; Unni, S. M.; Sreekumar, K.; Devi, R. N. Disordered Brownmillerite $Ba_2InCeO_{5+\delta}$ with Enhanced Oxygen Reduction Activity. *Chem. Mater.* **2012**, *24*, 2823−2828.

(2) Kaukonen, M.; Krasheninnikov, A. V.; Kauppinen, E.; Nieminen, R. M. Doped Graphene as a Material for Oxygen Reduction Reaction in Hydrogen Fuel Cells: A Computational Study. *ACS Catal.* **2013**, *3*, 159−165.

(3) Valim, R. B.; Santos, M. C.; Lanza, M. R. V.; Machado, S. A. S.; Lima, F. H. B.; Calegaro, M. L. Oxygen reduction reaction catalyzed by ε-MnO2: Influence of the crystalline structure on the reaction mechanism. *Electrochim. Acta* **2012**, *85*, 423−431.

(4) Savinell, R. F. Oxygen-Reduction Catalysts: Picking perovskites. *Nat. Chem.* **2011**, *3*, 501−502.

(5) Narayanamoorthy, B.; Datta, K. K. R.; Eswaramoorthy, M.; Balaji, S. Improved Oxygen Reduction Reaction Catalyzed by Pt/Clay/Nafion Nanocomposite for PEM Fuel Cells. *ACS Appl. Mater. Interfaces* **2012**, *4*, 3620−3626.

(6) Liu, X.; Meng, C.; Han, Y. Defective Graphene Supported MPd_{12} (M = Fe, Co, Ni, Cu, Zn, Pd) Nanoparticles as Potential Oxygen Reduction Electrocatalysts: A First-Principles Study. *J. Phys. Chem. C* **2013**, *117*, 1350−1357.

(7) Son, D. N.; Takahashi, K. Selectivity of Palladium−Cobalt Surface Alloy toward Oxygen Reduction Reaction. *J. Phys. Chem. C* **2012**, *116*, 6200−6207.

(8) Viswanathan, B.; Rao, C.; Varadaraju, U. V. Noble metal based anodes for polymer electrolyte membrane fuel cells. *Photo/Electrochem. Photobiol. Environ., Energy Fuel* **2006**, 43−101.

(9) Adzic, R. R.; Wang, J. X. Configuration and Site of O_2 Adsorption on the Pt(111) Electrode Surface. *J. Phys. Chem. B* **1998**, *102*, 8988−8993.

(10) Lu, M.; Kharkwal, S.; Ng, H. Y.; Li Sam, F. Y. Carbon nanotube supported MnO_2 catalysts for oxygen reduction reaction and their applications in microbial fuel cells. *Biosens. Bioelectron.* **2011**, *26*, 4728−4732.

(11) Morozan, A.; Jousselme, B.; Palacin, S. Low-platinum and platinum-free catalysts for the oxygen reduction reaction at fuel cell cathodes. *Energy Environ. Sci.* **2011**, *4*, 1238−1254.

(12) Poux, T.; Napolskiy, F. S.; Dintzer, T.; Kerangueven, G.; Istomin, S. Ya.; Tsirlina, G. A.; Antipov, E. V.; Savinova, E. R. Dual role of carbon in the catalytic layers of perovskite/carbon composites for the electrocatalytic oxygen reduction reaction. *Catal. Today* **2012**, *189*, 83−92.

(13) Xu, J.; Gao, P.; Zhao, T. S. Non-precious Co3O4 nano-rod electrocatalyst for oxygen reduction reaction in anion exchange membrane fuel cells. *Energy Environ. Sci.* **2012**, *5*, 5333−5339.

(14) Zhang, C.; Yanagisawa, K.; Tao, H.; Onda, A.; Shou, T.; Kamiya, S. Oxygen Reduction Activity and Methanol Resistance of Ru-based Catalysts Prepared by Solvothermal Reaction. *Catal. Lett.* **2012**, *142*, 1128−1133.

(15) Sunarso, J.; Torriero, A. A. J.; Zhou, W.; Howlett, P. C.; Forsyth, M. Oxygen Reduction Reaction Activity of La-Based Perovskite Oxides in Alkaline Medium: A Thin-Film Rotating Ring-Disk Electrode Study. *J. Phys. Chem. C* **2012**, *116*, 5827−5834.

(16) Benbow, E. M.; Kelly, S. P.; Zhao, L.; Reutenauer, J. W.; Suib, S. L. Oxygen Reduction Properties of Bifunctional α-Manganese Oxide Electrocatalysts in Aqueous and Organic Electrolytes. *J. Phys. Chem. C* **2011**, *115*, 22009−22017.

(17) Reddington, E.; Sapienza, A.; Gurau, B.; Viswanathan, R.; Sarangapani, S.; Smotkin, E. S.; Mallouk, T. E. Combinatorial Electrochemistry: A Highly Parallel, Optical Screening Method for Discovery of Better Electrocatalysts. *Science* **1998**, *280*, 1735−1737.

(18) Chan, B. C.; Liu, R. X.; Jambunathan, K.; Zhang, H.; Chen, G. Y.; Mallouk, T. E.; Smotkin, E. S. Comparison of High-Throughput Electrochemical Methods for Testing Direct Methanol Fuel Cell Anode Electrocatalysts. *J. Electrochem. Soc.* **2005**, *152*, A594−A600.

(19) Welsch, F. G.; Stöwe, K.; Maier, W. F. Fluorescence-Based High Throughput Screening for Noble Metal-Free and Platinum-Poor Anode Catalysts for the Direct Methanol Fuel Cell. *ACS Comb. Sci.* **2011**, *13*, 518−529.

(20) Welsch, F. G.; Stöwe, K.; Maier, W. F. Rapid optical screening technology for direct methanol fuel cell (DMFC) anode and related electrocatalysts. *Catal. Today* **2011**, *159*, 108−119.

(21) Liu, J. H.; Jeon, M. K.; Woo, S. I. High-throughput screening of binary catalysts for oxygen electroreduction. *Appl. Surf. Sci.* **2006**, *252*, 2580−2587.

(22) Stöwe, K.; Dogan, C.; Welsch, F.; Maier, W. F. High-Throughput Optical Screening of Electrocatalysts for Fuel Cell Applications − Review and Present Developments. *Z. Phys. Chem.* **2013**, *227*, 561−593.

(23) Klonis, N.; Sawyer, W. H. Effect of Solvent−Water Mixtures on the Prototropic Equilibria of Fluorescein and on the Spectral Properties of the Monoanion. *Photochem. Photobiol.* **2000**, *72*, 179−185.

(24) Klonis, N.; Sawyer, W. H. Spectral Properties of the Prototropic Forms of Fluorescein in Aqueous Solution. *J. Fluoresc.* **1996**, *6*, 147−157.

(25) Alvarez-Pez, J. M.; Ballesteros, L.; Talavera, E.; Yguerabide, J. Fluorescein Excited-State Proton Exchange Reactions: Nanosecond Emission Kinetics and Correlation with Steady-State Fluorescence Intensity. *J. Phys. Chem. A* **2001**, *105*, 6320−6332.

(26) Lee, D. H.; Sung, H. J.; Han, D. W.; Lee, M. S.; Ryu, G. H.; Aihara, M.; Takatori, K.; Park, J. C. In Vitro Bioassay of Endotoxin Using Fluorescein as a pH Indicator in a Macrophage Cell Culture System. *Yonsei Med. J.* **2005**, *46*, 268−274.

(27) Wang, L.; Roitberg, A.; Meuse, C.; Gaigalas, A. K. Raman and FTIR spectroscopies of fluorescein in solutions. *Spectrochim. Acta, Part A* **2001**, *57A*, 1781−1791.

(28) Chen, G. Y.; Delafuente, D. A.; Sarangapani, S.; Mallouk, T. E. Combinatorial discovery of bifunctional oxygen reduction -water oxidation electrocatalysts for regenerative fuel cells. *Catal. Today* **2001**, *67*, 341−355.

(29) Rasooly, A.; Weisz, A. In Vitro Antibacterial Activities of Phloxine B and Other Halogenated Fluoresceins against Methicillin-Resistant Staphylococcus aureus. *Antimicrob. Agents Chemother.* **2002**, *46*, 3650−3653.

DOI: 10.1021/co500128m
ACS Comb. Sci. 2015, 17, 164−175

(30) Neckers, D. C. Review: Rose Bengal. *J. Photochem. Photobiol., A* **1989**, *47*, 1−29.
(31) Gan, X.; Liu, S.; Liu, Z.; Hu, X.; Cui, Z.; Wang, Y. Determination of carbazochrome by fluorescence quenching method. *Spectrochim. Acta, Part A* **2012**, *97*, 161−166.
(32) Mead, J. A. R.; Smith, J. N.; Williams, R. T. Studies in Detoxication: The Biosynthesis of the Glucuronides of Umbelliferone and 4-Methylumbelliferone and their use in fluorimetric determination of p-Glucuronidase. *Biochem. J.* **1955**, *61*, 569−574.
(33) Park, S. H.; Choi, C. H.; Koh, J. K.; Pak, C.; Jin, S.; Woo, S. I. Combinatorial High-Throughput Screening for Highly Active Pd−Ir−Ce Based Ternary Catalysts in Electrochemical Oxygen Reduction Reaction. *ACS Comb. Sci.* **2013**, *15*, 572−579.
(34) Scheidtmann, J.; Saalfrank, J. W.; Maier, W. F. Plattenbau - Automated Synthesis of Catalysts and Materials Libraries. *Studies in Surface Science and Catalysis*; Elsevier: Tokyo, 2003; Vol. *145*, pp 13−21.
(35) Mizukami, S.; Okada, S.; Kimura, S.; Kikuchi, K. Design and Synthesis of Coumarin-Based Zn^{2+} Probes for Ratiometric Fluorescence Imaging. *Inorg.Chem.* **2009**, *48*, 7630−7638.
(36) Masuda, T.; Muroya, Y.; Nakatani, N. Coumarin Constituents of the Juice Oil from Citrus hassaku and Their Spasmolytic Activity. *Biosci., Biotechnol., Biochem.* **1992**, *56*, 1257−1260.
(37) Seixas de Melo, J.; Fernandes, P. F. Spectroscopy and photophysics of 4- and 7-hydroxycoumarins and their thione analogs. *J. Mol. Struct.* **2001**, *565*−*566*, 69−78.
(38) Caselli, M.; Daniele, V.; Mangone, A.; Paolillo, P. Application of Multiple Linear Regression and Extended Principal-Component Analysis to Determination of the Acid Dissociation Constant of 7-Hydroxycoumarin in Water/AOT/Isooctane Reverse Micelles. *J. Colloid Interface Sci.* **2000**, *221*, 173−180.
(39) Levillain, P.; Fompeydie, D. Determination of Equilibrium Constants by Derivative Spectrophotometry. Application to the pK,s of Eosin. *Anal. Chem.* **1985**, *57*, 2561−2563.
(40) Fink, D. W.; Koehler, W. R. pH Effects on Fluorescence of Umbelliferone. *Anal. Chem.* **1970**, *42*, 990−993.
(41) Liu, J. H.; Jeon, M. K.; Woo, S. I. High-throughput screening of binary catalysts for oxygen electroreduction. *Appl. Surf. Sci.* **2006**, *252*, 2580−2587. Jeon, M. K.; Liu, J. H.; Lee, K. R.; Lee, J. W.; McGinn, P. J.; Woo, S. I. Combinatorial Search for Quaternary Methanol Tolerant Oxygen Electro- Reduction Catalyst. *Fuel Cells* **2010**, *10*, 93−98.

DOI: 10.1021/co500128m
ACS Comb. Sci. 2015, 17, 164−175